 FDMP, vol.15, no.1, pp.1-14, 2019

A Study on the Optimal Offset Distance Between a Welding Torch and the Infrared Thermometers

Tae-Jong Yun[1], Won-Bin Oh[1], Bo-Ram Lee[1], Joon-Sik Son[2] and Ill-soo Kim[1, *]

Abstract: Detection of weld defects using real-time monitoring and controlling algorithm is of the significant task in manufacturing industries due to the increased production and liability costs that result when weld defects are not identified early in the production cycle. Monitoring and controlling for robotic arc welding process employed should be reliable, flexible and cost-effective in non-clean, high-volume production environments. Also, the robotic welding system has been utilized a complex jigging and mechanical devices to move the workpiece which related to the stationary welding head for getting higher efficiency and lower costs. To develop the fully robotic welding system, people make use of their senses of sound and/or sight to collect welding information, and take the necessary corrective measurements to ensure the weld quality after processing is satisfactory. Therefore, it is really required that the monitoring and controlling algorithm of sensors for increasing effectiveness in the robotic welding process has been developed.

In this paper, bead-on-plate welding using an infrared thermography in the robotic GMA (Gas Metal Arc) welding process has been performed to study the effects of welding parameters on thermal profile characteristics and find the optimal offset distance which applied for monitoring and controlling of welding quality such as bead height. The analysis for correlation between temperature distributions at three offset distance and bead height which based on the regression analysis such as Standard Error of Estimate (SEE), the coefficient of correlation (R) and coefficient of determination (R^2) and (Predictive Ability of Model) has been done. The infra-red sensor is useful for monitoring the isotherm radii that arise during the robotic welding process and identifying bead height as welding quality.

Keywords: GMA welding, adaptive control, bead-on-plate joint, infrared thermometers, bead height.

1 Introduction

Since various sensors have widely been employed in industries and engineering, the role

[1] Department of Mechanical Engineering, Mokpo National University, 1666 Yeongsan-ro, Cheonggye-myeon, Muan-gun, Jeollanam-do, 58554, South Korea.

[2] Research Institute of Medium & Small Shipbuilding, 55, Daebuljugeo 3-ro, Samho-eup, Yeongam-gun, Jeollanam-do, 58457, South Korea.

[*] Corresponding Author: Ill-soo Kim. Email: ilsookim@mokpo.ac.kr.

FDMP. doi:10.32604/fdmp.2019.04759 www.techscience.com/fdmp

of sensors has become more important with increasing demand for the robotic welding systems. Also, the sensors employed in robotic arc welding system must detect the changes in weld characteristics and produce the output that is in some way related to the change being detected [Hohn and Holmes (1986)]. The requirements of a welding sensor are normally universal, durable, reliable, compact, non-wearing and maintenance-free [Richardson (1986)]. Nowadays, there is today no welding sensor available that satisfies all of these demands because each sensor has a limitation either on its design or application to robots. In addition, the sensor will provide information for control of welding operations. The direct sensor would monitor weld pool size, shape and temperature distribution of the examples of characteristics [Malin (1986)].

The demand for better control and sensing in welding has increased with automation and welding processes involving new and advanced materials. This requires precise control of the welding process to produce the desired weld with respect to productivity and quality. Consequently, there is a need for different technologies to control precisely the process with respect to the different welding operating parameters. In doing so, sensors play a crucial role as the major source of input to the control system that manage and control the behavior and output of the welding system [Garasic (2015); Gupta and Arora (2007); Cederberg (2004)]. Typical sensors for the robotic arc welding system are acoustic, infrared, optical sensors and on-line radiography. There have been various techniques and sensors employed to control the welding process. Sensors for adaptive control technologies can be classified with preview (optical, acoustic, ultrasonic and infrared sensing) and arc sensing, which are discussed below [Cook, Andersen and Barrett (1988)]. As one of the most useful sensors, a through-the-arc sensing is the most common model of the joint tracking system incorporated into commercial robotic Fwelding systems. The technique makes use of the welding electrode as a sensor to gather information regarding arc voltage and welding current in the welding joint. Deviations in the current value are monitored, and feedback signals are sent to the robot controller. This feedback is essentially the technique by which the welding torch is centered within the joint. To control the torch height above the joint, a preselected arc voltage which represents the desire welding electrode extension is programmed into the robot controller. Arc voltage measured at the welding electrode was fed back to adjust the torch height [Hanright (1986)]. Commercially available joint tracking systems of this type incorporate both joint guidance and height control [Agapakis, Katz, Koifman et al. (1986)]. These systems assure that the welding arc will stay in the root of the joint and maintain an optimal stand-off distance. The systems are however limited by the quantity and quality of information that can be obtained from the arc signal [Rutishauser, Gutow, Anderson et al. (1986)]. Remwick et al. [Remwick and Richardson (1983)] employed arc sensing to monitor the welding pool in the GTA (Gas Tungsten Arc) and proposed the concept of the algorithm controlling the weld pool as a sensing technique. Another application of arc sensing is the detection of the metal transfer in the GMA welding process [Hardt (1986)]. As the droplet transfer mode in the GMA welding process has a great effect on weld pool metallurgy, depth of bead penetration and solidification, Johnson et al. [Johnson, Carlson and Smartt (1989)] has attempted to correlate perturbations in the electrical arc signals with droplet transfer in order to detect the detachment of individual droplet and to distinguish the three transfer modes.

Optical sensing technology has been exploited for a number of applications for joint tracking, penetration control, arc length sensing and electrode extension in the GMA welding [Kraus (1988); Gonseth and Blanc (1983); Agapakis, Katz, Koifman et al. (1986); Deam (1989)]. The developed system was first investigated by Boillet et al. [Boillet, Cielo, Begin et al. (1985)] for scanning the weld path. A fiber optic bundle was employed to transmit the infrared radiation from the surface in front of weld pools to the signal processing unit. Kraus [Kraus (1988)] made use of the optical spectral radiometric/laser reflectance method to measure the weld pool surface temperature of SS 304, SS 316L and 8630 in the stationary GTA welding. One of the first real-time optical tracking systems was the coaxial viewing system employed for joint tracking and weld pool width control [Richardson (1986)]. In this technique, the imaging system is integrated into the welding torch.

Infrared sensing, the inherent attraction for the welding process, has however, had successful applications for the robotic weld control. Infrared thermography is capable of monitoring the plate temperature distribution, which provides information for seam tracking, identification of plate geometry faults, penetration control, contamination and microstructure formation. Typical output parameters which have been investigated are the cooling rate, discontinuity sensing, bead penetration, contamination, seam tracking and bead geometry. Ivica et al. [Ivica, Zoran and Maja (2015)] analyzed the most commonly used sensing systems in the modern welding industry, which nowadays includes robotic systems. Also, several characteristics, limitations and advantages of sensor systems are presented and mechanisms of action are briefly described. Furthermore, a low-cost infrared sensing system based on the analysis of the surface temperature distribution is proposed for monitoring the perturbations occurring during the aluminum alloy MIG welding process. A galvanometer scanner is employed in this real-time infrared sensing system to continually reflect the infrared energy to the point infrared sensor [Yu, Xu, Zhou et al. (2017)]. Sadek et al. [Sadek and Fernand (2010)] presented an evaluation of an infrared sensor for monitoring the welding pool temperature in a GTA welding process to develop a real-time system control. Bestard et al. [Bestard, Sampaio, Vargas et al. (2018)] proposed a system developed to stimulate a GMA welding conventional process and collect values of the arc variables, infrared thermography and weld bead geometry. Zondi et al. [Zondi, Tekane, Magidimisha et al. (2017)] have reported on the temperature history of the welding cycle in the nozzle-to-shell circumferential weld of the pressure vessel using IR thermography. Controlling of bead penetration was obtained through monitoring the minor axis and ellipse isotherms which were shown to be the most sensitive variables to study the change due to variations into joint penetration depth and thickness of the plate being welded.

The objective of this study is to determine of optimal offset distance between welding torch and infrared thermometers. To achieve the objective, a new algorithm that provided the weld final configuration and properties as output parameter for detecting temperature distributions in the vicinity of the weld zone in robotic arc welding process have been developed to find a relationship between process parameters and thermal image from infrared thermography, and finally to investigate the interrelationship between isotherm radii versus bead width.

2 Experimental works

A number of problems related to the robotic GMA welding process for automation include the modeling, sensing and control of the process. Statistically designed experiments that are based upon Taguchi technique reduce costs and give the required information about the main and interaction effects on the response factors. In this study, an infrared thermometer was employed to detect temperature distributions in the vicinity of the weld zone. Therefore, the infrared thermometer test should be performed for determining the optimal distance between welding wire and three infrared thermometers before the main experiment carried out.

Fig. 1 shows a schematic diagram for a distance between wire and infrared thermometers. Table 1 shows an experimental layout for calibration of infrared thermometer. All other parameters except these parameters under consideration were fixed. Welding parameters for calibration were chosen the upper and lower limit of design of matrix. D1, D2 and D3 mean a distance of three infrared thermometers from welding torch.

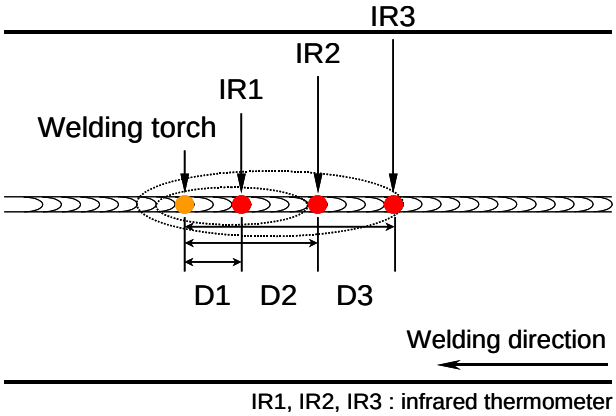

Figure 1: A schematic diagram for a distance between welding torch and infrared thermometers

Table 1: Experimental layout for calibration of infrared thermometer

Trial No.	C	V	S	D1	D2	D3
1	240	26	12	7	12	23
2	260	28	10	7	12	23
3	280	30	8	7	12	23
4	240	26	12	9	16	33
5	260	28	10	9	16	33
6	280	30	8	9	16	33

The experimental material for development of empirical equations was chosen 300×150×4.5 mm SS400 plates with bead-on plate joint in the robotic GMA welding process. The mechanical properties in base metal are shown in Table 2. In order to obtain

good welding quality, the oxide scale in the interface was removed firstly by stainless wire brush and sandpaper (#300). Fig. 2 shows a block diagram in the robotic GMA welding process for this study. The welding facility was chosen for the data collection and evaluation, Equipment to measure the distributions of the weld surface temperature was included infrared thermometers, arc monitoring system and desktop computer.

Table 2: Mechanical properties in base metal

Material	Tensile strength (kg/mm^2)	Yield point (kg/mm^2)	Elongation (%)	Impact value ($kg \cdot m/cm^2$)	Hardness (Hv)
SS400	43.5	32.5	25	6.2	128

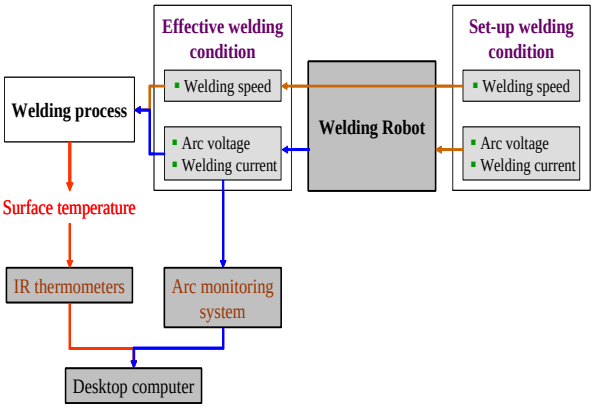

Figure 2: Block diagram in the robotic GMA welding process for this study

In the process of the experiments, the GMA welding unit employed in the experiment work is consisted of a robot control unit and a robot tech box. The torch positioning and motion control were achieved through monitoring the welding torch. With the welder and CO^2 shielding gas turned on, the robot was initialized and welding was then executed. Three infrared thermometers were employed to detect temperature in the vicinity of the weld pool. Although scanning infrared sensors are by far the most extensively used infrared for monitoring and controlling of the welding process, several intrinsic properties of these sensors have limited their practical industrial application. The infrared cameras are expensive, fragile in the harsh welding environment and require constant cooling using liquid nitrogen. Compared to infrared scanning cameras, infrared thermometers can be placed close to welding arc because of their compactness. Therefore, this type of sensor was employed in this work. As rapid temperature fluctuations about a true mean value can make the thermometer output unsuitable for recording and control, the average function was employed to provide a smoothed signal in this experiment.

$$A_0 = A_p + (M \pm A_p) \times 2\frac{\Delta T}{D} \quad (1)$$

A constant sensor position relative to the welding arc must be maintained during the welding process. A sensor attachment was constructed for easy adjustment of the sensor position relative to the weld centerline. This attachment ensured a constant sensor-to-plate surface distance was maintained even in the case of distorted plates and allowed the sensor to travel along the weld. To keep low-frequency, high-power electric noise from the welding power source from infiltrating the infrared thermometer signal line used optical fiber tube.

The data acquisition system was employed for measurement of temperature distributions. It consisted of a desktop computer, LabVIEW data acquisition card, output module. The output signals were controlling current signals from infrared thermometer. A Virtual Instruments (VI) controller was constructed to facilitate the control of welding parameters from the computer screen. With the acquisition system combined with the VI, the program could be obtained the acquired data, and output data were graphically displayed in real-time and could be saved into ASCII format for future analysis.

Experimental test plates were located in the fixture jig by the robot and the required weld conditions were fed for the particular weld steps in the robot path. With power supply and argon shield gas turned on, the robot was initialized and welding was executed. This continued until experimental runs were completed. To optimize the robotic GMA welding process, two samples were taken for observation after discarding 50 mm on each side to eliminate the end effects, and both surfaces were cleaned to take off dirt and oxides. Steel wire with diameters of 1.2 mm was employed as the welding consumables. Therefore, infrared thermometer test should be performed for determining the optical distance between welding wire and three infrared thermometers before main experiment carried out. The bead section after welding was cut transversely from the middle position using wire cutting machine to measure the bead width, and the incised specimen polished. A 3D scanner was used to measure precisely the bead width. After scanned bead width data, it was fitted by using commercial software called MATLAB. The experimental results were analyzed on the basis of relationship between welding parameters and bead height for robotic GMA welding process.

3 Results and discussion

3.1 Calibration of infrared thermometer position

Fig. 3 represents the bead geometry measured at the middle position for this study. Also, the measured bead geometry using 3D scanner for calibration experiments have been represented in Fig. 4. It was shown that the highest temperature distributions were measured at offset distance between welding torch and 1st infrared thermometer (D1), while the lower temperature variations observed at offset distance between 2nd and 3rd infrared thermometers (D2, D3). Besides, change of temperature fluctuation was increased as offset distance increased. As shown in Fig. 3, temperatures were not measured at 33 mm offset distance exactly. It can be confirmed that surface temperature

distributions reduce fast as the welding speeds increase so that the measured temperatures are unstable at great distance from welding torch.

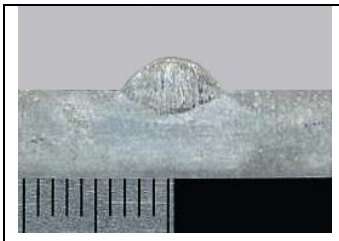	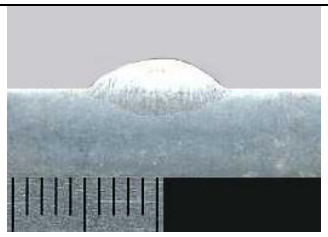	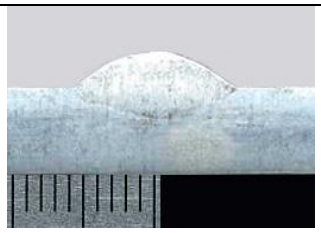
Trial No. 1	Trial No. 2	Trial No. 3
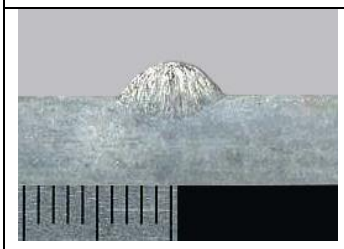	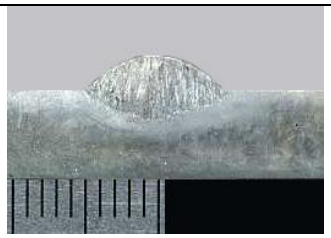	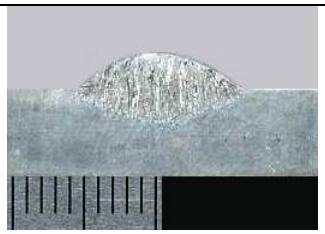
Trial No. 4	Trial No. 5	Trial No. 6

Figure 3: The bead geometry measured

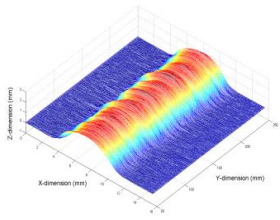	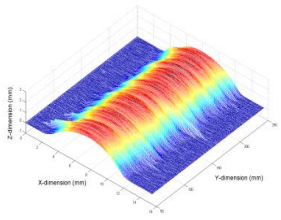	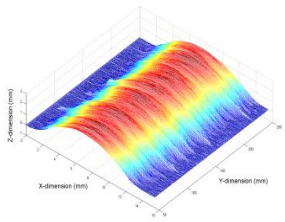
Trial No. 1	Trial No. 2	Trial No. 3
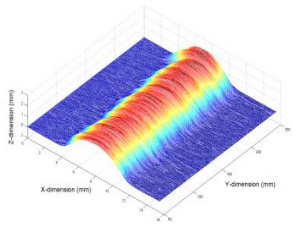	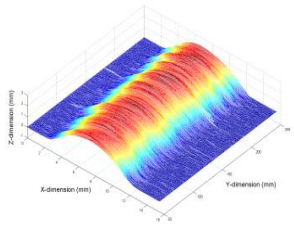	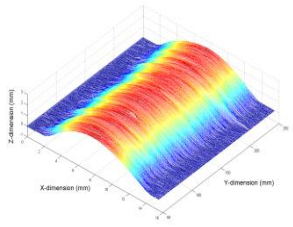
Trial No. 4	Trial No. 5	Trial No. 6

Figure 4: The measured bead geometry using 3D scanner for calibration experiment

3.2 Optimal offset distance

In order to determine optimal offset distance between welding torch and infrared thermometers, the mathematical models to study relationship between the measured temperature distributions and bead height have been developed. For the analysis of correlation, it was used the Standard Error of Estimate (SEE), coefficient of correlation (R) and coefficient of determination (R^2). Where SEE is used to identify an accuracy of the estimated values, R is the value to represent correlation between temperature distributions and bead geometry, R^2 is a coefficient to indicate an accuracy of regression equation. SEE, R and R^2 can be represented as follow;

$$SEE = \frac{\sigma}{\sqrt{N}} \tag{2}$$

$$R = \sqrt{\frac{SSR}{SSR}} \tag{3}$$

$$R^2 = \frac{SSR}{SST} \tag{4}$$

Where Sum of Squared Regression (SSR) is quantity that a factor expresses a depended variable as sum of square for factor, Sum of Squared Total (SST) is quantity that total plus Sum of Squared Error (SSE) and SEE is quantity that a cause excluded factors, expresses a depended variable.

In order to use that a value has a good correlation between temperature distributions and bead height, mean temperature distributions have been compared as the same way that distance analyzed. Tab. 3 shows the results of analysis for correlation between temperature distributions and bead height. Usually, in case R^2>0.65, regression model can be considered good correlation between factor and depended on variable. As shown in Tab. 3, temperature distributions at 9mm had a good correlation with bead height more than temperature variations at 7mm so that the optimal value was the minimum value in D1. In case of D2, temperature distributions at 12 mm and 16 mm had similar correlation with bead height, but R^2 of temperature distributions at 12mm for bead height was smaller than that of 0.65. Temperature variations at 33mm in D3 had not correlation with bead height because all R^2 values were smaller than 0.65. Temperature distributions at 23 mm in D3 were that minimum value is shown best value.

To compare performance of the models, the target was evaluated by PAM (Predictive Ability of Model) defined by Poliak [Poliak (1998)] as expressed in the following formula:

$$PAM = \frac{N_{PAM}}{N_{Total}} \times 100 \tag{5}$$

Where NPAM is the predicted value of range $\left|\frac{B_m \quad B_P}{B_m}\right| \leq 0.1$.

Table 3: The regression analysis results of temperature distributions for bead height

Symbol	Distance(mm)	R	R^2	Standard error of estimate
D1	7 mm	0.408	0.166	0.13677
	9 mm	0.850	0.722	0.07957
D2	12 mm	0.777	0.603	0.09436
	16 mm	0.839	0.704	0.08206
D3	23 mm	0.798	0.637	0.09029
	33 mm	0.712	0.507	0.10602

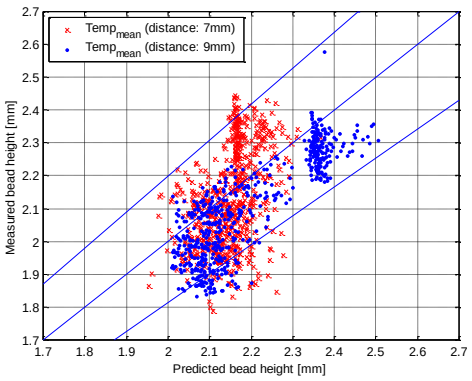

Figure 5: Comparison of the predicted and measured bead height at D1

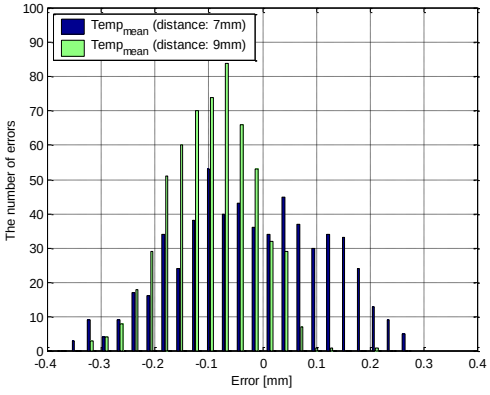

Figure 6: The error of the predicted bead height for at D1

Table 4: Analysis results for D1 point

Distance	Temperature characteristics	PAM(%)	Standard deviation
7mm	Mean	89.1709	0.1366
9mm	Mean	90.0169	0.0799

Fig. 5 shows correlation between temperature distributions and bead height at D1. In Fig. 5, the solid line represents the best fit, and the dotted line means over 90% predicted values. Temperature distributions have good correlation with bead eight when the predicted values are distributed concentrically to solid line. As shown in Fig. 5, temperature variations at 9 mm are concentrated more than that at 7 mm. Maximum temperature variations do not express bead with as shown in Fig. 5. The error of predicted bead width at D1 in order to identify performance of predicted equation through analysis of distribution of error represents Fig. 6. It was shown that temperature distributions at 9 mm presented more accuracy than that at 7mm for bead width. For bead height, temperature variations at 7 mm and 9 mm appeared similar results. Also comparisons of temperature distributions at 7 mm and 9 mm have been performed in Tab. 4 with PAM and standard deviation. As shown in Tab. 4, temperature at 9 mm appeared a good agreement more than that at 7 mm for bead height. In PAM, it cannot select optimal values from mean values. Therefore, the temperature distributions with the least values in standard deviation and chosen minimum value at 9 mm were chosen.

In order to determine optimal point of infrared thermometer at D2, correlation between temperature distributions and bead height was represented in Fig. 7. As shown in Fig. 7 both temperature distributions at 12 mm and 16mm had a good correlation with bead height, because relationship between temperature distributions and bead height is linear mostly. The error of predicted bead width at D2 to identify performance of predicted equation through analysis of distribution of error represents Fig. 8 As shown in Fig. 8, the temperature variations at 7 mm and 9 mm for bead height appeared similar results. Also comparisons of temperature distributions at 12 mm and 16 mm have been performed in Tab. 5 with PAM and standard deviation. The results shown in Tab. 5.was indicated the similar trends. As all kinds of temperature distributions without classification by distance and data processing had a similar correlation with bead height, searching of optimal point was very difficult. Therefore, several facts in order to determine optimal point of infrared thermometer at D2 should be considered. Therefore, 16 mm as the optimal point of infrared thermometer at D2 was determined.

Fig. 9 represents correlation between temperature distributions at D3 and bead height. As shown in Fig. 9, distributions of predicted bead height are presented like a perpendicular line which, means that temperature variations at 33 mm didn't predict bead height according to a change of welding condition. Distribution of error at 23mm is closer to 0 than that of a 33 mm as shown in Fig. 10. Tab. 6 describes temperature at 23 mm appeared a good agreement more than that at 33mm for bead height. Therefore, it should be concluded that optimization is minimum temperature at 23 mm. From the previous analysis results, the offset distance for D1, D2 and D3 on main experiment used is determined 9, 16, 23 mm respectively.

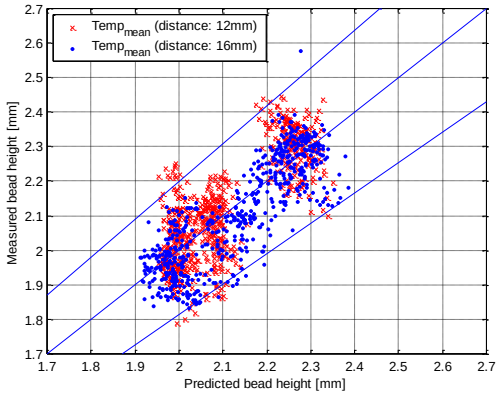

Figure 7: Comparison of the predicted and measured bead height at D2

Table 5: Analysis results for D2 point

Distance	Temperature characteristics	PAM(%)	Standard deviation
12 mm	Mean	95.2623	0.0943
16 mm	Mean	96.9543	0.0823

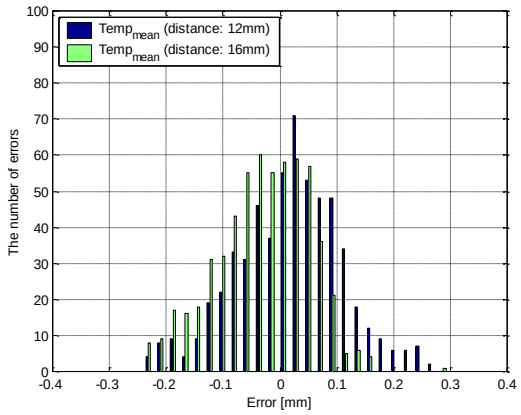

Figure 8: The error of the predicted bead height for at D2

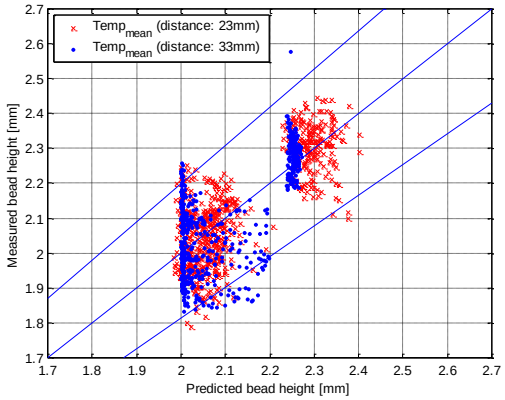

Figure 9: Comparison of the predicted and measured bead height at D3

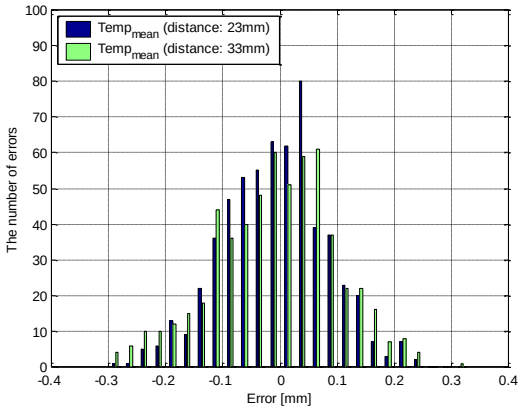

Figure 10: The error of the predicted bead height for at D3

Table 6: Analysis results for D3 point

Distance	Temperature characteristics	PAM(%)	Standard deviation
23mm	Mean	97.1235	0.0902
33mm	Mean	93.2318	0.1066

4 Conclusions

From the observation of robotic arc welding process and isotherm radii measured using an infrared thermography, bead-on-plate welding was conducted on 16 specimens with a change of process parameters such as welding current, welding speed and arc voltage. Thermal distributions were measured using infrared thermography during the robotic GMA welding process. According to the results of analysis for thermal distribution,

thermal distributions have changed with bead height. For correlation between temperature distributions at three offset distance and bead height which based on the regression analysis such as Standard Error of Estimate, coefficient of correlation, coefficient of determination and PAM method, the new algorithm has been developed. Since in case R^2>0.65, regression model can be considered good correlation between factor and depended variable, the optimal offset distance for D1, D2 and D3 on main experiment employed is determined 9, 16, 23 mm respectively. Since the developed algorithms are able to predict process parameters required to achieve desired bead width and to establish guidelines and criteria for the most effective joint designs, adaptive control using infrared thermography may be achieved with the development of appropriate computer interface with both the welder control and the technique used for infrared thermography.

Acknowledgement: This work was supported by the Project of Technology Development for Industry Core (No. 20002772, Smart Logistics & Production Automation System for Pipe Spool, Steel Out- Fitting and Block Logistics in Shipbulding and Offshore Platform) funded By the Ministry of Trade, Industry & Energy (MOTIE, Korea) References.

References

Agapakis, J. E.; Katz, J. M.; Koifman, M.; Epstein, G. N.; Friedman, J. M. et al. (1986): Joint tracking and adaptive robotic welding using vision sensing of the weld joint geometry. *Welding Journal*, vol. 65, no. 11, pp. 33-41.

Agapakis, J. E.; Katz, J. M.; Koifman, M.; Epstein, G. N.; Friedman, J. M. et al. (1986): Joint tracking and adaptive robotic welding using vision sensing of the weld joint geometry. *Welding Journal*, vol. 65, no. 11, pp. 33-41.

Alfaro, S. C. A.; Fernand, D. F. (2010): Exploring infrared sensoring for real time welding defects monitoring in GMAW. *Sensor*, vol. 10, pp. 5972-5973.

Bestard, A. V.; Sampaio, R. C., Vargas, A. R.; Alfaro, S. C. (2018): Sensor fusion to estimate the depth and width of weld bead in real time in GMAW processes. *Sensor*, vol. 18, no. 4, pp. 962-968.

Boillet, J. P.; Cielo, P.; Begin, G.; Michel, C.; Lessard, M. et al. (1985): Adaptive welding by instrumental considerations. *Welding Journal*, vol. 64, no. 7, pp. 209-217.

Cederberg, P. (2004): *On Sensor-Controlled Robotized One-off Manufacturing (Ph.D. Thesis).* Lund University, Sweden.

Cook, G.; Andersen, E. K.; Barrett, R. J (1988): Feedback and adaptive control in welding. *Proceedings of the 2nd International Conference on Trends in Welding Research*, pp. 891-903.

Deam, R. T. (1989): Weld pool frequency: a new way to define a weld procedure. *Recent Trends in Welding Science and Technology: TWR `89: Proceedings of the 2nd International Conference on Trends in Welding Research*, pp. 967-971.

Garašić, I. (2015): Sensors and their classification in the fusion welding technology.

Sensors and Their Division in Welding Technology, vol. 22, no. 4, pp. 1069-1074.

Gonseth, P. M.; Blanc, P. (1983): Optiguide-a new optical joint tracking device. *Welding Journal*, vol. 62, no. 9, pp. 27-29.

Gupta, A. K.; Arora, S. K. (2007): *Industrial Automation and Robotics*. Laxmi Publications, New Delhi.

Hanright, J. (1986): Robotic arc welding under adaptive control-A survey of current technology. *Welding Journal*, vol. 65, no. 11, pp. 19-24.

Hardt, D. E. (1986): Measuring weld pool geometry from pool dynamics. *Modeling and Control of Casting and Welding Processes: Proceedings of the 3rd Conference on Modeling of Casting and Welding Processes*, pp. 3-17.

Hohn, R. E.; Holmes J. G. (1986): Robotic arc welding adding science to the art. *Robotic Welding a Guide to Selection and Application, SME Publications*, pp. 14-25.

Ivica, G.; Zoran, K.; Maja, R. (2015): Sensors and their classification in the fusion welding technology. *Technical Gazette*, vol. 22, pp. 1069-1074.

Johnson, J. A.; Carlson, N. M.; Smartt, H. B. (1989): Detection of metal trasfer mode in GMAW. *Recent Trends in Welding Science and Technology: TWR `89: Proceedings of the 2nd International Conference on Trends in Welding Research*, pp. 337-181.

Kraus, H. G. (1988): Experimental measurement of weld pool temperatures-a review. *Modeling and Control of Casting and Welding Processes Ⅳ: Proceedings of the 4th International Conference on Modeling of Casting and Welding Processes*, pp. 205-212.

Kraus, H. G. (1988): Experimental measurement of weld pool temperatures-a review. *Modeling and Control of Casting and Welding processes Ⅳ: Proceedings of the 4th International Conference on Modeling of Casting and Welding Processes*, pp. 205-212.

Malin, V. (1986): Problems in design of integrated welding automation-Part 1: Analysis of welding related operations as objects for welding automation. *Welding Journal*, vol. 65, no. 11, pp. 53-60.

Poliak, E. I. (1998): Application of linear regression analysis in accuracy assessment of rolling force calculations. *Metals and Materials*, vol. 4, no. 5, pp. 1047-1056.

Remwick, R. J.; Richardson, R. W. (1983): Experimental investigation of GTA weld pool oscillation. *Welding Journal*, vol. 62, no. 2, pp. 29-35.

Richardson, R. W. (1986): Robotic weld joint tracking systems-theory and implementation methods. *Welding Journal*, vol. 65, no. 11, pp. 43-51.

Richardson, R. W.; Gutow, A.; Anderson, R. A.; Farson, D. F. (1984): Coaxial weld pool viewing for process monitoring and control. *Welding Journal*, vol. 63, no. 3, pp. 43-50.

Yu, P.; Xu, G.; Zhou, G.; Tian, Y. (2017): A low-cost infrared sensing system for monitoring the MIG welding process. *International Journal of Advanced Manufacturing Technology*, vol. 92, pp. 4031-4038.

Zondi, M. C.; Tekane, Y.; Magidimisha, E.; Wium, E.; Gopal, A. et al. (2017): Characterization of submerged arc welding process using infrared imaging technique. *Journal of South Africa Institution of Mechanical Engineering*, vol. 33, pp. 66-74.